



([www.anm2015.com](http://www.anm2015.com))

## ANM Abstracts

Abstracts in session ANM for Plenary, Invited, Oral and Poster presentations

### Contents

Page	Abstract No	Title
1	102	Microstructural Properties of ZnO Powder Nanostructures Prepared by Mechanical Alloying
2	106	Spin transport in poly(ferrocenylsilane) and the related polymers
3	107	Hydrogenation of silicene and its thermal stability
4	108	Characterization of a Water-In-Oil-In-Water Multiple Emulsion Integrating Biomimetic Aqueous-Core Lipid Nanoballoons Housing Protein Entities
5	109	Nanofiber materials for visible light driven simultaneous generation of NO and O <sub>2</sub> ( 1 Dg)
6	114	Controlled Freezing and Freeze-drying for Nanosized Oxide Ceramic...
7	116	Barium Titanate Nanoparticles - Micro-Raman Phase Transition Probe
8	124	Temperature Coefficient of Resistance of carbon nanotube/ Poly(Nisopropylacrylamide) composites for infrared and thermal sensing
9	127	High responsivity photodetector based on PbS QDs/Si heterostructure
10	128	Photoluminescence studies in Tm implanted Al <sub>x</sub> Ga <sub>1-x</sub> N layers
11	130	Gold and Palladium Gold Catalysts Used for Nitrate Reduction from Water
12	131	Laser ablation in liquids: a simple approach to produce nanophosphors
13	136	Synthesis and characterization of Na(Y/Gd)F <sub>4</sub> upconverting nanoparticles for multimodal imaging
14	138	Magnetic Behavioural Change of Silane Exposed Graphene Nanoflakes
15	139	Microbial toxicity test of functionalized iron-oxide nanoparticles for possible use in soil aquifer treatment system
16	140	Polymorphism of ciclopirox-olamine in mucoadhesive buccal films
17	143	Characteristics of ultrafine/nanocrystalline Ti-20Nb-5Ta alloy processed by severe plastic deformation
18	144	Crystallization Processes of Proteins and Small Organic Molecules
19	145	Immobilization in LBL Films of Chlorophyll Encapsulated in Liposomes –

76	294	Towards white light in nitrides through defect engineering
77	296	Nanocomposites Based on Thermosetting Polyurethane and Multi-Walled Carbonnanotubes with Surface Functionalization
78	298	Experimental set-up for generating nano-objects with stable concentrations used to validate measuring apparatus in real time
79	301	Water purification by chitosan-hydroxy apatite nano hybrid system
80	302	Vascular drug delivery system based on nano noisome
81	303	Structural characterization of Sr doped LaFeO <sub>3</sub> thin films prepared by pulsed electron deposition method
82	314	Development of a new TBC system for more efficient gas turbine engine application
83	318	Investigating the effect of nanofiller geometry on the elastic constants of metal-based nanocomposites: A molecular dynamics study
84	326	Magnetically-driven release of doxorubicin from hydroxyapatite nanoparticles
85	327	Covalent Antibody Immobilization on the Electrospun Nanofiber for High Sensitive Biosensor Applications
86	338	Determination of dustiness of nanomaterials with the rotating drum test method
87	345	A candidate for a multiple ReRAM using the Au/TiO <sub>2</sub> /Ti thin film
88	357	Intraband optical activity of a semiconductor nanocrystal
89	358	Ligands Effect in High Photoluminescence of CuInS <sub>2</sub> /ZnS quantum dots synthesis
90	359	Influence of Polyaniline as Coating on the NaNbO <sub>3</sub> /PVDF Composite Properties
91	360	SnO <sub>2</sub> Films-Based Varistor Prepared by Electrophoretic Deposition
92	370	An original route to target delivery via core-shell modification of SPIONs
93	377	Microwave solvothermal synthesis of nanocrystal Cu <sub>2</sub> ZnSnS <sub>4</sub> (CZTS) materials for photovoltaic applications
94	387	Influence of ligands on the electronic states of assembled CdSe nanocrystal hybrid films
95	389	One Dimensional Nanostructures Polymer Composite Electrodes and Photoactive Layers for Efficient, Stable and Flexible Organic Photovoltaic Devices
96	395	A model of molecular aggregation in semiconductor nanocrystals-tetrapyrrole molecules complexes
97	398	Electronic structure of CsPbI <sub>3</sub> /RbPbI <sub>3</sub> cation ordered superlattices
98	402	Gigantic enhancement in broadband photo detection of electrospun CoTiO <sub>3</sub> nanosensors
99	406	Magnetocaloric effect in La <sub>0.7</sub> Sr <sub>0.3</sub> MnO <sub>3</sub> nanohole arrays
100	408	Nanocrystalline Cu <sub>2</sub> ZnSnSe <sub>4</sub> Thin Films for Solar Cells Applications: Microdiffraction and Structural Characterization
101	409	Optical, Morphological and Structural Properties of Self-Organized TiO <sub>2</sub> Nanotubes for Sensor Applications
102	420	In-Situ Analysis of the Reduction of Supported Pt Catalysts Using UV-Vis-NIR Spectroscopy
103	425	Abinitio vibrational properties of the carbon-modifiedNowotnyphase Ti <sub>5</sub> Si <sub>3</sub>
104	428	Conductive and flexible materials containing graphene-DNA hybrids for

# Electronic structure of CsPbI<sub>3</sub>/RbPbI<sub>3</sub> cation ordered superlattices

Abdykadyrov Baurzhan<sup>1</sup> and Takibaev N. Zh.<sup>1</sup>

<sup>1</sup>Physics department, al-Farabi Kazakh National University, Kazakhstan, abkxat@gmail.com

## ANM-nanomaterial-Poster

### INTRODUCTION

Halide perovskites have recently emerged as promising materials for low-cost, high-efficiency solar cells[1]. Many studies have followed with the aim of both improving the performance of these materials in photovoltaic cells and of understanding which physical parameters may determine the efficiencies[2]. Good understanding of the structural and electronic properties is very important to predict new related functional materials.

### THEORETICAL STUDY

We have performed first principles density functional calculations of CsRbPb<sub>2</sub>I<sub>6</sub> halide perovskites with two different methods. The first approach is density functional calculations with the PBE-GGA approximation implemented in VASP [3]. The momentum space integrations were performed using a  $5 \times 4 \times 4$   $\Gamma$ -centered Monkhorst-Pack  $k$ -mesh [4]. For the various symmetries examined, the lattice constants and internal coordinates were fully optimized until the residual Hellmann-Feynman forces became smaller than  $10^{-6}$  eV/Å. Secondly, we have applied the hybrid density functional calculation of CRYSTAL09 [4] to study the electronic structure, especially to get the band gap energy.

### RESULTS AND DISCUSSION

Group theory analysis shows that  $\bar{a}\bar{a}c^+$  octahedral tilting stabilizes the  $Pmc2_1$  orthorhombic phase in the superlattice shown in Fig. 1(a). The large pink sphere represents a Cs ion and the small green sphere represents a Rb ions. PbI<sub>6</sub> octahedra linked in  $c$  axis and have significant distortion and tilting. The unit cell contains four formula unit for perovskite (20 atoms), and  $Pmc2_1$  space group is actually a polar space group.

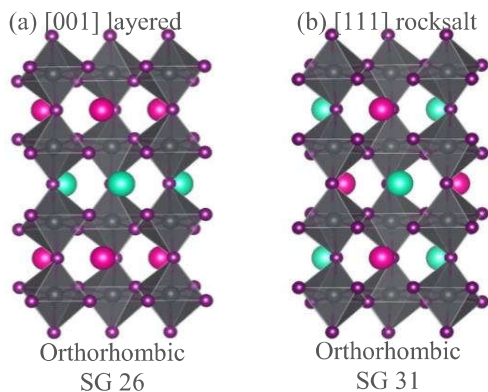


Figure 1. Structure of CsRbPb<sub>2</sub>I<sub>6</sub> superlattices in [001] and [111] directions

We show in table 1. structural and electronic properties of parent structures RbPbI<sub>3</sub>, CsPbI<sub>3</sub> and superlattices in [100], [110], [111] directions within PBE and PBE0 approximation. In [100] direction the band gap value is 1.892 eV and 2.68 eV respectively. In [110] direction the band gap value is 1.871 eV and 2.70 eV respectively. Electronic structure of superlattices in [111] direction shows band gap value is 1.885 eV and 2.63 eV respectively.

Structure	Volume (Å <sup>3</sup> )	Total E (eV)	E <sub>g</sub> PBE (eV)	E <sub>g</sub> PBE0 (eV)
RbPbI <sub>3</sub>	478.83	-28.202	1.922	2.86
CsPbI <sub>3</sub>	503.13	-28.358	1.822	2.57
CsRbPb <sub>2</sub> I <sub>6</sub> [001]	490.86	-28.271	1.892	2.68
CsRbPb <sub>2</sub> I <sub>6</sub> [110]	491.46	-28.266	1.871	2.70
CsRbPb <sub>2</sub> I <sub>6</sub> [111]	491.28	-28.269	1.885	2.63

Table. 1 Structural and electronic properties of RbPbI<sub>3</sub>, CsRbI<sub>3</sub> and CsRbPb<sub>2</sub>I<sub>6</sub>.

### CONCLUSION

We have examined the structural and electronic properties of ferroelectric compound CsRbPb<sub>2</sub>I<sub>6</sub>. We find the ground states of structures of the [100] and [111] ordered superlattices are polar. In all three directions the band gap value of PBE is underestimates ~70 % compared to that PBE0 hybrid functional calculation.

### REFERENCES

1. Wan-Jian Yin, Ji-Hui Yang, Joongoo Kang, Yanfa Yan, Su-Huai Wei, J. Matter. Chem A (2014)
2. Ball, J. M., Lee, M. M., Hey, A., Snaith, H. J., Energy Env. Sci., 6 (2013)
3. G Kresse, J Furthmuller, VASP-Guide (2003)
4. H.J. Monkhorst, J.D.Pack, Phys. Rev. B, 13 (1976)
5. R. Dovesi, V.R. Saunders, CRYSTAL09 User's Manual (2013)